SUPER-RESOLUTION IMAGING OF PRESYNAPTIC ACTIN: DISTINCT ACTIN NANOSTRUCTURES IN BEAD-INDUCED AND NATURAL PRESYNAPSES

CHANNA ELISE JAKOBS

Abstract

Neurons are responsible for signal transmission throughout the nervous system. This information transmission occurs at the synapse, where neurotransmitter passes from the presynaptic to the postsynaptic compartment. Actin filaments are abundantly present at the synapse. While the postsynaptic actin structure and function are well studied, presynaptic actin stays behind due to imaging difficulties that are caused by the dense actin cluster in the postsynapse that overshadows the presynaptic actin. Recently, the Leterrier lab used polylysine-coated beads to induce isolated presynapses and discovered that they contain three distinct actin nanostructures: (1) an actin mesh at the active zone, (2) actin rails between the active zone and the deeper parts of the presynapse, and (3) actin corrals that surround the presynapse. Using this bead-induced presynaptic model, we found that the actin mesh, rails, and corrals are present at actin enriched, actin non-enriched, excitatory, and inhibitory bead-induced presynapses. Moreover, we confirmed the existence of these actin nanostructures in 'natural' synapses that are formed between an axon and a dendrite, using CRISPRCas9 techniques to endogenously tag β-actin and single molecule localization microscopy (SMLM). This novel and unique combination of techniques allowed us to observe the presynaptic actin structure in 'natural' synapses, that was not observed before.

Supervisors
Dr. Christophe Leterrier
Dr. Nael Nadif Kasri

Affiliation
Radboud University, Nijmegen, The Netherlands

Introduction

Neurons are polarized cells that are responsible for the transmission of information in the nervous system (Gentile et al., 2022; Kevenaar & Hoogenraad, 2015). They have a large network of branched dendrites to receive information from other neurons and one axon that is responsible for transmitting the integrated information to target cells. This information transmission occurs at the synapse where chemical neurotransmitters pass from the presynaptic to the postsynaptic compartment. Decades of research have aimed to unravel the complex architecture of both the pre- and postsynaptic sides of the synapse (Südhof, 2021). One important component that is abundantly present in synapses is filamentous actin, one of the three major cytoskeletal proteins (Leterrier et al., 2017). That actin filaments serve an important role in the functioning of neurons is shown in for example animal research: defects in the actin cytoskeleton are associated with pathologies such as Fragile X Syndrome (Klemmer et al., 2011) and Parkinson's Disease (Sousa et al., 2009).

The function and structure of postsynaptic actin filaments are well studied on a cellular level. Here, actin serves a role in the organization and trafficking of receptors and regulation of the spine shape (Cingolani & Goda, 2008; Gentile et al., 2022). There are three interconnected and highly dynamic actin filament clusters found in the postsynapse: (1) a branched actin cluster in the spine head, (2) linear and branched actin structures in the neck of the spine, and (3) a linear actin cluster at the base of the spine (Dillon & Goda, 2005; Korobova & Svitkina, 2010; Star et al., 2002). On the other hand, the role of presynaptic actin filaments has remained difficult to pinpoint. Moreover, results in the existing literature are contradictory. Studies that are aiming to unravel the function of presynaptic actin filaments found that introduction of agents to downregulate polymerization of actin filaments either lead to an increased vesicle mobility, have no effect, or inhibit neurotransmitter release (Cingolani & Goda, 2008; Gentile et al., 2022; Wu & Chan, 2022). Genetic interference with actin filament polymerization, by creating a knock-out of different isoforms of actin monomers (β- and γactin), showed that actin filaments also play an important role in endocytosis: the β- or γ-actin knockout showed inhibited endocytosis at Calyx of Held and hippocampal synapses (Wu et al., 2016).

To unravel the function of presynaptic actin filaments it is important to delineate its architecture by imaging its organization. Actin filaments are thin (approximately 6 nm) and form dense structures (Leterrier, 2021a). Classical light microscopy has a diffraction limit of approximately 200 nm (Jacquemet et al., 2020), making it hard to observe the refined actin structure. For example, to investigate the actin structure in the axon shaft, where it appears as rings with a periodicity of 180- 190 nm (Leterrier, 2021b; Xu et al., 2013), the diffraction limit fails to reveal this periodicity (Figure 1B). The development of super-resolution microscopy allows to resolve structures that are smaller than the diffraction limit. One example of super-resolution microscopy is single molecule localization microscopy (SMLM; Figure 1). This technique is based on the localization of single molecules. A single emitter's intensity has a Gaussian shape, called the point spread function (PSF; Figure 1A). Consequently, by fitting a Gaussian function over a single emitter, one can determine its location at a resolution of approximately 20 nm (Jacquemet et al., 2020).

Two emitters from which the PSF do not overlap can be individually localized. In SMLM the PSFs of single emitters are temporally separated. The distance between the structure that is imaged and the fluorophore, called the linkage error, is among others a limiting factor in SMLM for the resolution, making the choice of labelling strategy crucial (Lelek et al., 2021).

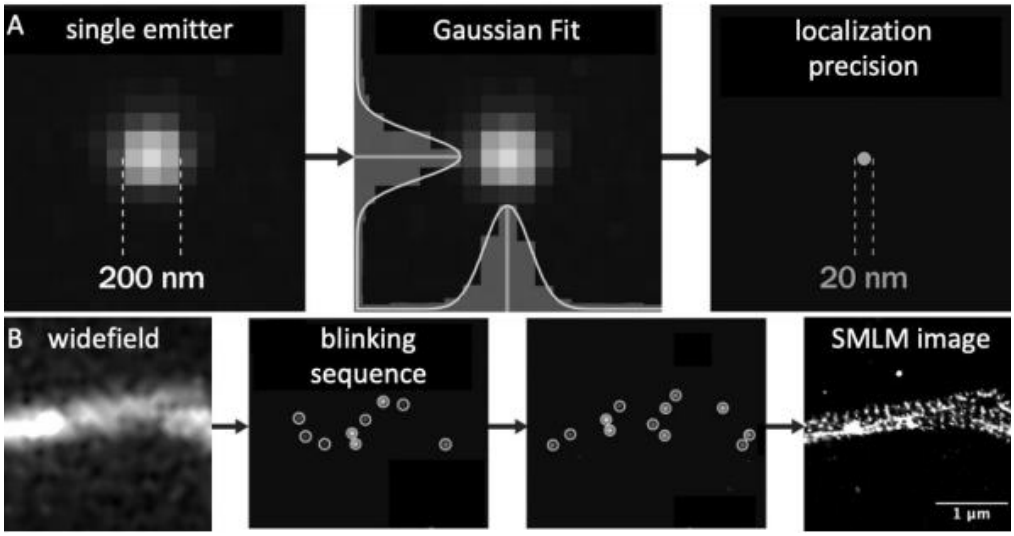

Figure 1. Principle of single molecule localization microscopy (SMLM): SMLM reveals periodic (180-190 nm) actin rings in axon shaft. (A) Diffraction limited image of a single emitter, showing the diffraction limit of approximately 200 nm (left panel). Fitting a Gaussian over the diffraction limited image of emitter (center panel), to determine the emitter's location with a precision of approximately 20 nm. (B) Diffraction limited (total internal reflection, TIRF) image of actin in the axon shaft, stained with phalloidin-Alexa Fluor 647 Plus (left panel). During an SMLM acquisition thousands of frames are collected, all displaying a different blinking pattern (middle panels). These frames are reconstructed into an SMLM image (right panel; STORM image of the same region as displayed in the left panel with actin labelled with phalloidin-Alexa Fluor 647 Plus). Adapted from Jimenez et al. (2020).

An emitter can be either in a 'bright' state, where it emits light, or in a 'dark' state, where it does not emit light. Going from the dark state into the bright state, and back into the dark state is called a 'switching cycle' or 'blinking' (Figure 1B). In stochastic optical reconstruction microscopy (STORM) blinking is caused by photoswitchable synthetic fluorophores in the presence of a buffer that forces the fluorophores into the dark state (Lelek et al., 2021; Rust et al., 2006). Irradiation of the sample with a laser causes fluorophores to blink stochastically. In another form of SMLM, called PAINT (point accumulation in nanoscale topography), blinking is caused by fluorophores that are immobilized by binding to their target (Jimenez et al., 2020; Lelek et al., 2021). These fluorophores subsequently detach from their target and diffuse freely through the buffer. Once the fluorophore is immobilized it is detected by a camera as a blinking event. In a particular form of PAINT, called DNA-PAINT, DNA oligonucleotides are used as 'imager strands' that could recognize a 'docking strand' that is bound to the target of interest. The imager strand is coupled to a fluorophore. In order to obtain a high quality SMLM image, one should pay attention to factors as (1) the signal-to-noise ratio, because of its susceptibility to background, (2) a sufficient amount of blinking to obtain a good reconstruction of the structure, however the blinking must not be too dense to separate the PSFs, and (3) photobleaching, because acquisitions are rather long and require a high laser power.

SMLM methods such as STORM are used to observe fine actin filament structures as the earlier described ring periodicity of actin in axon shafts (Figure 1B), but also presynaptic actin filaments. However, the presence of the densely packed apposed postsynaptic actin filaments 'overshadows' the presynaptic actin filaments (Korobova & Svitkina, 2010; Zhang & Benson, 2002). This makes it impossible, even when using SMLM, to observe presynaptic actin filaments (Figure 2). In a recent preprint by Bingham et al. (2022) presynaptic actin was imaged using a model to induce presynapses in the absence of the actin-rich postsynaptic compartment. Beads coated with poly-D-lysine were seeded on neuronal cultures (Lucido et al., 2009). At the contact points between a bead and an axon, the coated bead induced clustering of presynaptic proteins and led ultimately to the formation of functional presynaptic boutons that are competent for synaptic vesicle cycling. By creating presynapses devoid of postsynapses, the bead-induced presynapse model overcomes the problem of presynaptic actin being hidden by the postsynaptic actin cluster.

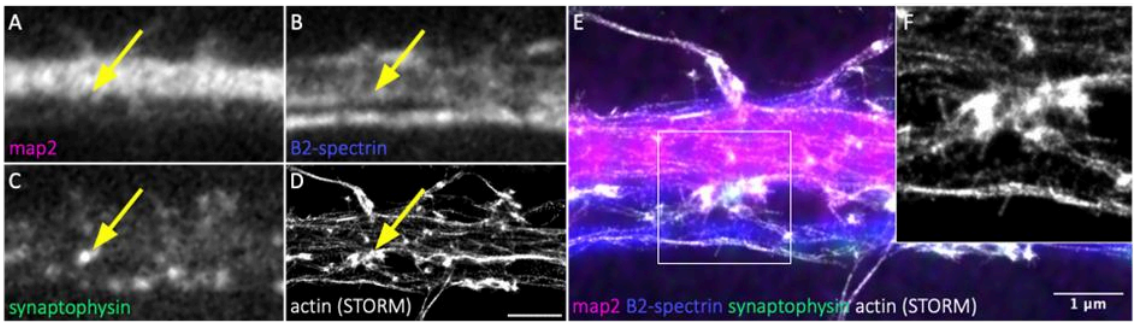

Figure 2. Imaging of presynaptic actin is hindered by a dense and vast postsynaptic actin cluster. Diffraction limited images of (A) map2, (B) b2-spectrin, and (C) synaptophysin. (D) STORM image of actin labelled with phalloidin-Alexa Fluor 647 Plus. Scale bar = 2 mm. (E) Overlay of the diffraction limited and STORM images with a (F) 2,5 x 2,5 mm zoom of the synapse.

Using STORM imaging of actin in these bead-induced presynapses, Bingham et al. (2022) found that there are three distinct actin nanostructures present in the presynapse: (1) an actin mesh in contact with the bead, where the active zone of synaptic vesicle exocytosis is located, (2) actin rails between the active zone and the deeper part of the presynapse, where the reserve pool (RP) of synaptic vesicles is located, and (3) peri-synaptic actin corrals that surround the whole presynapse, separating it from the axon shaft (Figure 3). Identification of these distinct nanostructures allows to hypothesize about the function of actin at presynapses. The actin mesh at the active zone may for example hinder exocytosis (Li et al., 2018), whereas the actin corrals in the periphery may play a role in the maintenance of the RP by acting as a scaffold protein (Sankaranarayanan et al., 2003). The rails may be important for synaptic vesicle trafficking from and to the RP (Sakaba & Neher, 2003). However, one should pay attention to the fact that these structures are found in a model. To be able to speculate about the function of actin in 'natural' synapses that are formed between neurons, it is necessary to observe the presynaptic actin structure in 'natural' synapses.

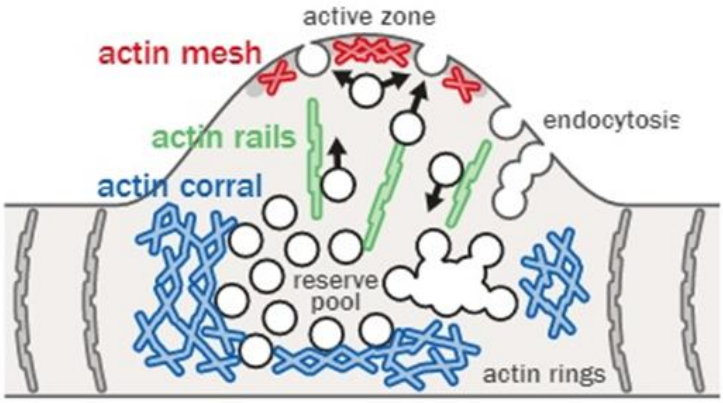

Figure 3. Schematic representation of presynaptic actin nanostructures. An actin mesh (red) at the active zone, actin rails (green) between the active zone and the deeper part of the synapse, and an actin corral surrounding the presynapse. From Bingham et al. (2022).

As pointed out in the paper by Bingham et al. (2022), actin enrichment is associated with different concentrations of other presynaptic components and a higher rate of vesicular cycling. Additionally, there are known molecular differences between excitatory and inhibitory synapses (Favuzzi & Rico, 2018). Poly-D-lysine coated beads can induce both inhibitory and excitatory synapses, which distinguishes them from other models such as neuroligin-induced presynapses (Lucido et al., 2009). This thesis aims to determine if the three actin nanostructures that are found by Bingham et al. (2022) are present in actin enriched, actin non-enriched, excitatory, and inhibitory synapses, or if there is a difference in the presynaptic actin structure between those different synapse types. It is found that the actin mesh, rails, and corrals are present in actin enriched, actin non-enriched, excitatory and inhibitory bead-induced synapses, suggesting that actin organizes similarly in all these different synapse categories. Furthermore, this thesis aims to confirm that the three types of actin nanostructures also exist in 'natural' synapses that are formed between two neurons, rather than between a coated bead and a neuron. We optimized different labelling strategies to image endogenously tagged actin and were able to confirm the existence of the nanostructures in 'natural' synapses.

Methods

Animals and cell culture

The animals and cell culture are handled according to the same protocol as in Bingham et al. (2022). In short, pregnant female Wistar rats (Janvier labs) were sacrificed and the hippocampal neurons of the E18 embryos were cultured. 18 mm diameter round coverslips were provided with paraffine dots and treated with poly-L-lysine. Three hours after seeding with neurons, the cells were transferred (cells facing down) to a petri dish containing a confluent glial cell culture and kept in neurobasal+ medium (supplemented with 2% B-27, 100 UI/mL penicillin/streptomycin, and 2.5 µg/mL amphotericin).

Preparation of poly-D-lysine coated beads

Aliphatic amine latex beads (3 mm diameter, Thermo Fisher) were incubated for 3 hours with poly-D-lysine (Sigma) and Dulbecco's phosphate buffered saline (D-PBS) at room temperature on a wheel to agitate. After incubation, the beads were washed two times with Volvic water and one time with neurobasal+.

The washed beads were diluted in neurobasal+, to determine the optical density (OD). After measuring the OD the bead solution was further diluted to adjust the bead quantity to 3.000.000 beads/coverslip. The bead solution was seeded dropwise onto 7 days in vitro (DIV7) neuronal culture (cells facing up). After 3 hours the coverslips were flipped, so that the neurons were facing the astrocytes again. Two days later (DIV9) the neurons were fixed and further handled.

CRISPR-mediated knock-in via transfection

While we waited for the adeno-associated viruses (AAVs) to be made, we used transfection to generate knock-in cells. Plasmids and AAVs containing the Cas9, donor (Table 1), and single guide RNA (sgRNA) sequences were produced in the NeuroCyto Lab. The donor sequence was designed to be linear DNA, using a HiUGE system (Gao et al., 2019), that was in frame with the actin sequence. Thus, the Cas9/sgRNA complex cuts exactly in frame in the donor sequence and the actin gene (ORF1), resulting in the insertion of the tag at the actin N-terminus. At DIV6, 700 ng DNA and 1 mL lipofectamine 2000 (Invitrogen) were both diluted in 25 mL neurobasal medium in separate tubes and incubated for 5 minutes at room temperature. Subsequently, the two dilutions were put together, gently mixed, and incubated for 20 minutes at room temperature. The mix was then added dropwise to the cultured cells on the coverslip in a 12-well plate with 450 mL neurobasal medium (cells facing up), and incubated at 37°C, 5.0% CO2. After 30 minutes of incubation, the coverslips were put back into their original medium, facing the astrocytes, until further experimenting.

CRISPR-mediated knock-in via viral infection

AAV particles were obtained from plasmids by co-transfection with a helper and packaging plasmid in producing cell lines (HEK 293T). At DIV0 cells were infected with the three constructs. Coverslips were put in a 12-well plate in 400 mL neurobasal+ that was supplemented by a 24-hour incubation on a glial cell culture (conditioned medium; cells facing upward). The constructs were diluted in conditioned neurobasal+ medium (109 viral particles/100 mL for each AAV) and added dropwise to the 400 mL medium in the 12-well plate. After two days, the coverslips were put back into their original medium (cells facing down to the glial cells).

Tag	Sequence	Reference
ALFA	SRLEEELRRRLTE	Götzke et al., 2019
FLAG	DYKDDDDK	-
GFP	237 amino acids	-
HA	YPYDVPDYA	-
Spot	PDRVRAVSHWSS	Proteintech, n.d., Virant et al., 2018
ALFA-FLAG	[ALFA] ... [FLAG]	Götzke et al., 2019
3X ALFA	[ALFA] ... [ALFA] ... [ALFA]	Götzke et al., 2019

Table 1. Sequences that were used to tag the β-actin using CRISPR-Cas9 gene-editing technique. All sequences were inserted at a locus corresponding to the N-terminus of β-actin.

Immunocytochemistry and sample preparation

DIV9 cells were fixed for 10 minutes at room temperature with 4% paraformaldehyde (PFA) + 4% sucrose in PEM (PIPES 80 mM, MgCl2 2 mM, EGTA 5 mM in H2O; pH 6.8). Subsequently, cells were rinsed 3 times at room temperature with 0.1 M phosphate buffer (TpO4), blocked and permeabilized for 1 hour at room temperature in immunocytochemistry (ICC: TpO4, gelatin 0.22%, Triton 0.1%) buffer, and incubated with primary antibodies and/or nanobodies in ICC buffer overnight at 4°C in a humidified dark box. For an overview of the primary antibodies and nanobodies that are used see Table 2.

Structure	Primary antibody/nanobody	Supplier	Reference	Dilution
	Antibodies (target, species, IgG type)			
Dendritic marker	map2 chicken IgY	Synaptic Systems	188 006	1/1000
Neuronal marker	β2-spectrin mouse IgG1	Abcam	-	1/100
	α2-spectrin mouse IgG2b	Ozyme BioLegend	BLE 803201	1/100
Presynaptic marker	synaptophysin1 guinea pig	Synaptic Systems	101 004	1/300
	bassoon mouse IgG2a	Abcam	ab82958	1/150
	munc 13-1 rabbit	Synaptic Systems	126 103	1/400
	vgat rabbit	Synaptic Systems	131 003	1/1000
	vglut guinea pig	Synaptic Systems	135 304	1/500
Actin	ALFA mouse IgG1	NanoTag	N1582	1/200
	aGFP rabbit	Abcam	ab82958	1/500
	HA mouse IgG1 Alexa Fluor 647	ThermoFisher	26183-A647	1/500
	HA rat	Roche	-	1/200
	FLAG mouse IgG1	Sigma	F3265	1/500
	Nanobodies (target, conjugation, application)			
Actin	ALFA-Alexa Fluor 647, STORM	NanoTag	N1502	1/50
	ALFA-docking strand 3, DNA-PAINT	Massive Photonics	-	1/100
	GFP-Alexa Fluor 647, STORM	NanoTag	N0304-af647-L	1/50
	GFP-docking strand 3, DNA-PAINT	Massive Photonics	-	1/50
	Spot-Alexa Fluor 647, STORM	ChromoTek	ebAF647-10	1/200
	ALFA-docking strand F3, -Atto 488, DNA-PAINT	Massive Photonics	-	1/200

Table 2. Primary antibodies and nanobodies that are used for immunostaining.

The next day, the coverslips are washed 3 times with ICC buffer, after which they were incubated with the corresponding secondary antibodies diluted in ICC buffer for 1 hour at room temperature (for an overview of the secondary antibodies that are used see Table 3). Subsequently, they were rinsed 3 times with ICC buffer and 3 times with TpO4. After these washes, coverslips were either kept in TpO4 with sodium azide (1/400) at 4°C, or further prepared as described below.

For the bead experiments the coverslips were incubated with phalloidin-Alexa Fluor 647 Plus (1/400, 165 nM; Thermo Fisher) in TpO4 for 72 hours and mounted in a silicone chamber before imaging (Jimenez et al., 2020). For epifluorescence imaging, the coverslips were mounted on Prolong Glass (PLG; Invitrogen). The anti-ALFA-Alexa Fluor 647 nanobody was not put with the primary antibodies overnight. After the three rinses with ICC buffer, these samples were incubated for 10 minutes with NGS buffer (normal goat serum: PBS, 10% NGS, 0.1% Triton), incubated with the ALFA-Alexa Fluor 647 nanobody in NGS for 1 hour at room temperature, and rinsed with TpO4.

Samples containing nanobodies were postfixed, if not mounted on PLG, for 5 minutes in 2% PFA in TpO4 at room temperature, rinsed with TpO4, and then put in TpO4 with sodium azide (1/400).

Secondary antibody	Conjugation	Supplier	Reference	Dilution
Goat-anti-chicken	DyLight 405	Rockland (TébuBio)	603-146-126	1/400
Donkey-anti-mouse IgG	Alexa Fluor 488	ThermoFischer	A21202	1/400
Goat-anti-mouse IgG1	Alexa Fluor 488	ThermoFischer	A21121	1/400
	Alexa Fluor 555		A21127	1/400
	Alexa Fluor 647		A21240	1/300
Goat-anti-mouse IgG2b	Alexa Fluor 488	ThermoFischer	A21141	1/400
	Alexa Fluor 555		A21147	1/400
Donkey-anti-rabbit	Alexa Fluor 555	ThermoFischer	A31572	1/400
Donkey-anti-guinea pig	Alexa Fluor 555	ThermoFischer	A21434	1/400
Goat-anti-rat	Alexa Fluor 647	ThermoFischer	A21247	1/300

Table 3. Secondary antibodies that are used for immunostaining.

Epifluorescence microscopy

Epifluorescence images were taken with an Axio-Observer upright microscope (Zeiss), with a 63X NA 1.4 objective and an Orca-Flash4.0 camera (Hamamatsu). A z-stack was obtained of either 8 or 9 slices that were spaced 0.21 mm. From this z-stack the slice that was most in focus was used for the figure.

Single Molecule Localization Microscopy

STORM imaging of the bead-induced presynapses were performed on an N-STORM microscope from Nikon Instruments. An Agilent MLC-400B laser launch with 405 nm (50 mW maximum fiber output power), 488 nm (80 mW), 561 nm (80 mW), and 647 nm (125 mW) solid-state lasers was used in the setup, with a 100X NA 1.49 objective and an Ixon DU-897 camera (Andor). Samples were mounted in a silicone chamber that was filled with STORM buffer (Jimenez et al., 2020; 1/2000, 30 nM phalloidin-Alexa Fluor 647 Plus, Smart Buffer Kit from Abbelight: 100 mM mercaptoethylamine (MEA), 3% glucose oxidase (GLOX) solution).

After a region of interest was found, a total internal reflection (TIRF) image was acquired (647 nm laser power: 0.5%, exposure time: 50 ms). Subsequently, the 3D STORM image was acquired (60.000 frames, exposure time: 15 ms, 647 nm laser power: 100%, 256x256 pixels). Reactivation of the fluorophores was performed during the acquisition using low-power 405 nm laser illumination.

STORM imaging of the endogenously tagged actin samples was performed at the same setup as described before. The sample was also mounted the same way, only the concentration of the MEA differed: 50 mM, and there was no phalloidin-Alexa Fluor 647 Plus in the buffer. When a region of interest was found, a TIRF image was acquired with the same settings as described before, after which the 3D STORM image was acquired (60.000-100.000 frames, exposure time: 15-30 ms, 647 nm laser power: 50-100%, 256x256 pixels). While acquiring reactivation of the fluorophores was performed by an increased illumination with the 405 nm laser.

DNA-PAINT was performed on the same N-STORM microscope setup as STORM. Samples were mounted in an open chamber with PAINT buffer (Imaging Buffer, Massive Photonics) with 0.125-1 nM imager strands coupled to Atto 655 (I3) or Atto 643 (F3). When a region of interest was found, the PAINT image was acquired (60.000-100.000 frames, exposure time: 30-50 ms, 647 nm laser power: 50-80%, 256x256 pixels).

STORM and PAINT image postprocessing

Both STORM and PAINT images were postprocessed using DECODE, a deep-learning algorithm that localizes single emitters in a sample that shows dense blinking with better accuracy than other postprocessing software (Speiser et al., 2021). The obtained localizations were then transformed into ThunderSTORM files (Ovesný et al., 2014). The transformed localizations were drift corrected using the SMAP module in MATLAB (Ries, 2020). Images were reconstructed and 4x4 mm zooms of regions of interest were made using Fiji (Schindelin et al., 2012), scripts and macros that were developed by the NeuroCyto Lab (https://github.com/cleterrier/ChriSTORM).

Image quantification, analysis and statistics

Presence/absence of the actin nanostructures in bead-induced presynapses. 4x4 mm zooms were scored by visual inspection as ‘present’, ‘absent’, or ‘undefined’ for the three actin nanostructures (mesh, rails, corral). A structure was scored as undefined when it could not be reliably determined if the structure was either present or absent. The actin mesh is defined as a small cluster of actin at the contact of the bead with the axon. Linear structures within the synaptic bouton are defined as rails. Corrals are defined as large actin clusters distal from the active zone, surrounding the presynaptic bouton. The percentage of all scored synapses that showed the actin mesh, rails or corral was calculated. Fisher’s exact test of independence was used to determine if there were significant differences between the actin enriched and non-enriched bead-induced synapses. This test was performed in RStudio (RStudio Team, 2020). Significance was defined as: ns = not significant, * = $p < .05$, ** = $p < .01$, and *** $p < .001$. nsynapse represents the number of scored synapses.
Actin mesh and corral size in bead-induced presynapses. For the bead-induced presynapses that are scored with an actin mesh and/or corral, the surface of these structures was carefully outlined in 2D reconstructions using Fiji (Schindelin et al., 2012). A polygon selection was drawn around the borders of the actin structures, and the area was measured. The total surface per bead-induced presynapse of the mesh and the corral was calculated.

The data of the actin enriched bead-induced presynapse mesh ($p = .0023$) and corral ($p = 0.0090$) size was not normally distributed (Shapiro-Wilk test, performed in Prism9, GraphPad Software). Therefore, the whole dataset was treated as not normally distributed (actin-non enriched mesh $p = .1207$, actin non-enriched corral $p = .1308$). A Mann-Whitney test was performed using Prism9 (GraphPad Software). Significance was defined as: ns = not significant, * = $p < .05$, ** = $p < .01$, and *** $p < .001$. nsynapse represents the number of scored synapses.

Results

Actin nanostructures are present in both actin enriched and non-enriched bead-induced presynapses.

While Bingham et al. (2022) found that approximately 70% of the bead-induced presynapses is enriched in actin and 30% is non-enriched, it remains unclear if this variation in enrichment affected the actin nanostructures. Therefore, we first aimed at reproducing these findings while differentiating between actin enriched and actin non-enriched bead-induced presynapses. Diffraction limited images of bead-induced presynapses were judged as either actin enriched (nsynapse = 14) or actin non-enriched (nsynapse = 11), by visually comparing the intensity of the presynaptic actin staining compared to the surrounding part of the axon (Figure 4A&B). Subsequently, super-resolved images of these presynapses were scored for the presence or absence of the actin mesh, rails, and corrals (Figure 4C). The percentage of scored presynapses that displayed the actin mesh, rails or corral was calculated (Figure 4D). There was no difference found: the mesh ($p = 1$), rails ($p = .6766$), and corrals ($p = 1$) were present in the same number in both actin enriched and actin non-enriched bead-induced presynapses (Fisher's exact test of independence). This suggests that the actin nanostructures occur in both synapse types, independently of the actin concentration.

While scoring the bead-induced presynapses for the presence or absence of the nanostructures, we noticed that the actin corrals in the actin enriched bead-induced presynapses seemed bigger than in the non-enriched bead-induced presynapses. To quantitatively assess if the size of the structures differs between actin enriched and non-enriched bead-induced presynapses, we carefully measured the size of the mesh and corrals for each presynapse (Figure 4E, see methods for measurement protocol). Quantification of the rails is more difficult because these structures are very thin. Besides, we do not expect that these thin structures will contribute to the enhanced actin intensity in the diffraction limited images. Therefore, we excluded the rails from the quantification. There was no difference in the size of the mesh between actin enriched (nsynapse = 12) and actin non-enriched (nsynapse = 9) bead-induced presynapses ($p = .9881$), but there was a significant difference in the surface of the corrals ($p = .0286$; nsynapse actin enriched = 12; nsynapse actin non-enriched = 10): the corral in the actin enriched bead-induced synapses are bigger than the corral in the non-enriched bead-induced synapses (Mann-Whitney test). This suggests that the difference in actin enrichment between actin enriched and non-enriched is driven by an increased or decreased size of actin corrals at the presynapse, respectively.

Nanostructures are present in both excitatory and inhibitory synapses.

The poly-D-lysine coated bead-induced presynapse model can induce both excitatory and inhibitory presynapses. This made it interesting to investigate whether the actin nanostructures are present in both excitatory and inhibitory bead-induced presynapses. Excitatory and inhibitory bead-induced synapses were identified by looking at the presence of either vGluT (vesicular glutamate transporter that loads synaptic vesicles with glutamate; stains excitatory synapses) or vGAT (vesicular GABA transporter that loads synaptic vesicles with GABA and glycine; stains inhibitory synapses) staining in diffraction limited images (Südhof, 2021; Figure 5A, C).

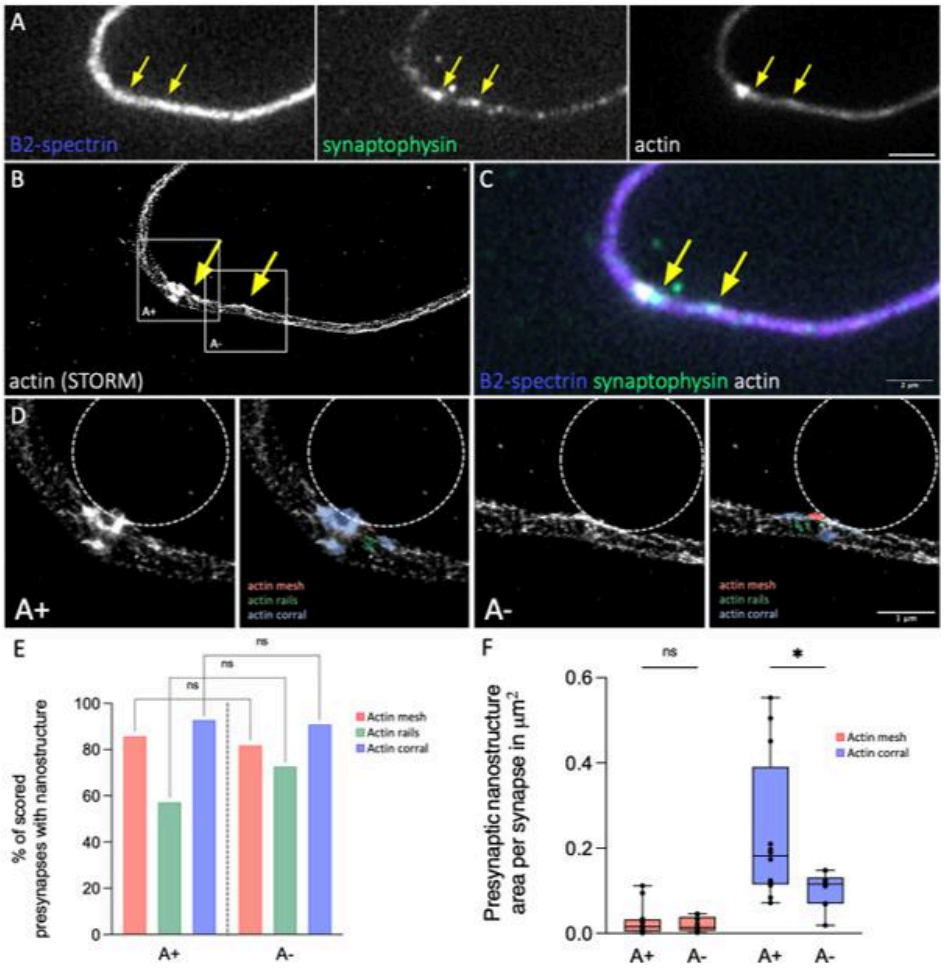

Figure 4. Three distinct nanostructures present in both actin enriched (A+) and actin non-enriched (A-) bead-induced presynapses. (A) Diffraction limited images of b2-spectrin (purple), synaptophysin (green) and actin (white; scale bar = 4 mm), and (B) STORM image of actin labelled with phalloidin-Alexa Fluor 647 Plus. (C) An overlay of the diffraction limited images. The left and the right arrow indicate an A+ and A- bead-induced presynapse respectively. (D) 4x4 mm zooms of the A+ and A- bead-induced presynapses that are indicated in image (B). The dashed circle in the zoom indicates the location of the bead. In the second and the fourth zoom the actin mesh (red), rails (green), and corrals (blue) are indicated. (E) Bar graph of the percentage of scored presynapses that showed the actin mesh (red), rails (green), or corrals (blue) in A+ (left) or A- (right) bead-induced presynapses. Fisher's exact test of independence, ns $p > .05$. (E) Boxplot of the area of presynaptic mesh (red) or corral (blue) per A+ or A- bead-induced synapse in µm2. Dots reflect individual data points. Mann-Whitney test, ns $p > .05$, * $p < .05$.

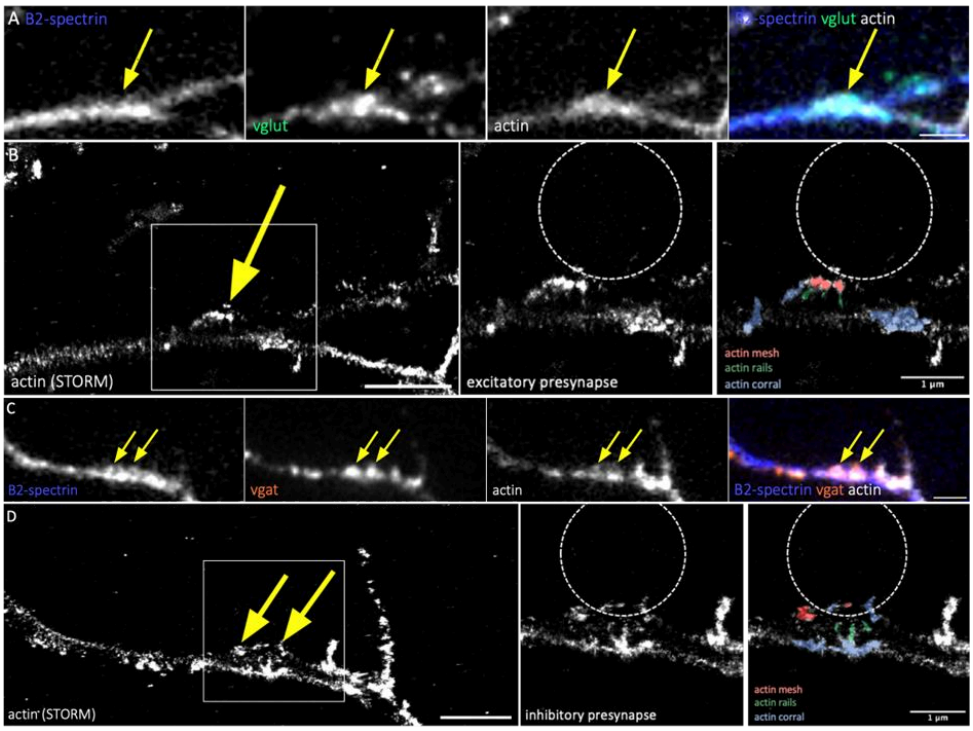

Figure 5. Three distinct nanostructures present in both excitatory and inhibitory bead-induced presynapses. (A&C) Diffraction limited images of b2-spectrin (purple), vGluT (A; green) or vGAT (C; orange), and actin (white), and an overlay of the three images. The arrows indicate the bead-induced presynapses. (B&D) STORM images of actin labelled with phalloidin-Alexa Fluor 647 Plus. The right two images are the 4x4 mm zooms of the bead-induced presynapses that are indicated in the left image. The dashed circle in the zoom indicates the location of the bead. In the second zoom the actin mesh (red), rails (green), and corrals (blue) are indicated. Scale bars = 2 mm.

Super-resolution imaging of actin within 'natural' presynapses using knock-in GFP-actin neurons: distinct actin nanostructures are not visible.

After having validated that the three actin nanostructures are present in actin enriched, actin non-enriched, excitatory, and inhibitory bead-induced presynapses, we wanted to confirm that these nanostructures are also present in 'natural' synapses that are formed between an axon and a dendrite. To observe presynaptic actin in a 'natural' synapse, it must be imaged in the absence of the dense postsynaptic actin structure. To overcome this problem, CRISPR-Cas9 gene-editing was used to endogenously tag b-actin (Nishizono et al., 2020). Transfection or infection of cultured neurons resulted in only a small number of cells on the coverslip having the tag inserted into their genome, resulting in the formation of synapses between a knock-in neuron and a non-knock-in neuron (Figure 6). To obtain the best image of the presynaptic actin structure, different labelling strategies were tested, optimized, and imaged.

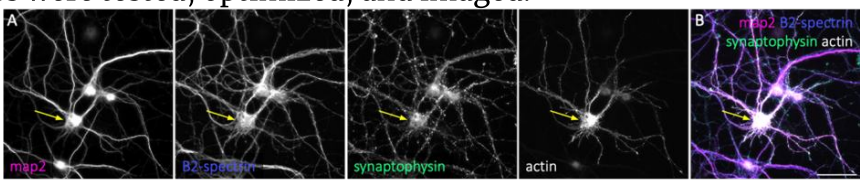

Figure 6. Not all cells on a coverslip are expressing endogenously tagged actin, using CRISPR-Cas9. (A) Diffraction limited images of map2 (magenta), b2-spectrin (purple), synaptophysin (green), and ALFA-actin labelled with an anti-ALFA nanobody-Alexa Fluor 647 (white). (B) An overlay of the four images. The arrow indicates the cell that is expressing the endogenously tagged actin. Scale bar = 50 mm.

β-actin was tagged with GFP to observe synapses between the axons of a knock-in neuron, and the dendrite of a non-knock-in neuron. An anti-GFP primary antibody with the appropriate secondary coupled to Alexa Fluor 647 was used to observe the actin-GFP with STORM (Figure 7A, B&C). Figure 7C displays a presynapse of a knock-in neuron, with a dendritic counterpart from a non-knock-in neuron. Close inspection of the presynaptic actin-GFP structure did not result in identification of the actin nanostructures that are found in the bead-induced presynaptic model. This might suggest that the actin nanostructures are specific to the bead model. However, the periodic actin rings were also not visible (Figure 7C), suggesting that the labelling strategy was sub-optimal. The use of the GFP-tag that is 237 amino acids long in combination with a primary and secondary antibody might result in a linkage error that is too big to observe the actin nanostructures (de Beer & Giepmans, 2020). Besides, the primary-secondary complex might also hinder the accessibility of neighboring binding sites, resulting in too little antibodies on the actin structure to reconstruct the actin nanostructures.

To reduce the linkage error and overcome the problem of hinderance of neighboring binding sites, a nanobody was used (de Beer & Giepmans, 2020). The actin-GFP was labelled with a nanobody anti-GFP that was coupled to docking strand 3, making it suitable for DNA-PAINT (Figure 7D, E&F). The autofluorescence of the GFP-tag was used to identify knock-in neurons. Again, close inspection of the DNA-PAINT image did not result in identification of the actin nanostructures. Together with the absence of neighboring axonal actin rings, this suggested that the labelling strategy again does not allow to observe enough detail. Each imager strand only has one fluorophore, whereas secondary antibodies have multiple fluorophores. It might be that the blinking density was too low to obtain a detailed reconstruction of the actin nanostructure. Another explanation might be that the linkage error that is caused by the 237 amino acids long GFP-tag resulted in too little detail to observe the actin nanostructures.

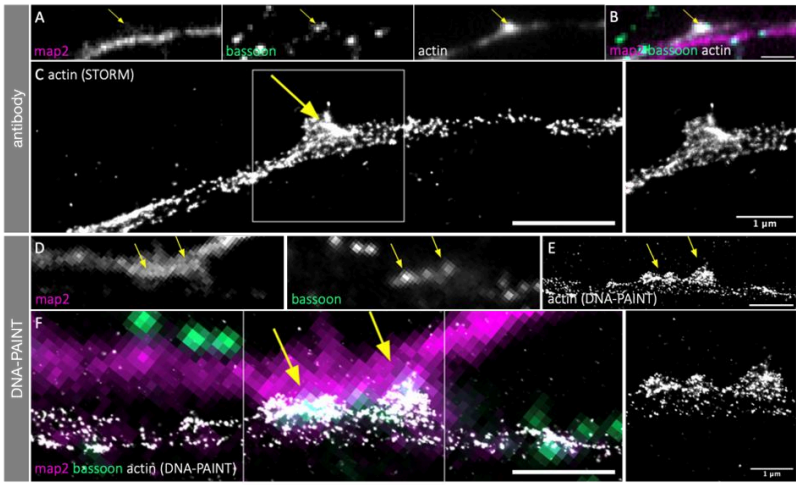

Figure 7. Distinct nanostructures are not visible in GFP-actin presynapses labelled with a primary and secondary antibody or a DNA-PAINT nanobody. (A) Diffraction limited images of map2 (magenta), bassoon (green), and actin (white), and (B) an overlay of the three images. The arrow indicates a presynapse of a knock-in (KI) neuron that is formed with a dendrite from a non-KI neuron. (C) STORM image of actin that is endogenously tagged with GFP. GFP is labelled with an anti-GFP primary antibody with the appropriate secondary antibody coupled to Alexa Fluor 647. The zoom on the right is indicated in the left image. (D) Diffraction limited images of map2 (magenta) and bassoon (green). (E) DNA-PAINT image of actin that is endogenously tagged with a GFP. GFP is labelled with a nanobody anti-GFP that is coupled to docking strand 3, and the I3 imager coupled to Atto 655. (F) An overlay of the three images. On the left a zoom of the DNA-PAINT image is displayed. This zoom is indicated in the left image. Scale bar = 2 mm.

Super-resolution imaging of actin within 'natural' presynapses using knock-in ALFA-actin neurons: distinct nanostructures are visible.

To reduce the linkage error that is caused by the GFP-tag and favor the accessibility to the tags, smaller endogenous tags were tested. b-actin was tagged with an ALFA- (Götzke et al., 2019), HA-, or Spot-tag (Proteintech, n.d.; Virant et al., 2018). We were unable to obtain images of sufficient quality with the HA- and Spot-tag (data not shown), while this was possible with the small ALFA-tag (13 amino acids) after optimization of the labelling strategy. A nanobody anti-ALFA coupled to Alexa Fluor 647 was used to stain the ALFA-tag (Figure 8A, B&C). After optimizing the immunocytochemistry protocol, the number of blinking events per image was too low to identify actin structures as for example the periodic actin rings in the axonal shaft (Leterrier, 2021b; Xu et al., 2013; Figure 8C). This was due to an abrupt drop in blinking events per frame during the first half of the acquisition. Unstable binding by nanobodies to their target is a known limit in using nanobodies (Traenkle & Rothbauer, 2017). However, one would expect a gradual decrease in blinking events per frame, and not the abrupt decrease that we observed during the imaging of the anti-ALFA nanobody. The abrupt drop in blinking might be caused by bleaching of the fluorophore. As described in the method section, the fluorophores are reactivated by low power 405 nm laser illumination. This makes that the amount of blinking per frame stable throughout the first part of the acquisition. However, when the drop in number of blinking events per frame took place, the 405 nm laser illumination was not able to compensate for the progressive bleaching of the fluorophore anymore. Conclusively, the performance of the nanobody was insufficient to image the actin nanostructure in the presynapse.

Another labelling strategy was tried to overcome the limits of the anti-ALFA nanobody. An anti-ALFA primary antibody was used in combination with the appropriate secondary antibody coupled to Alexa Fluor 647 (Figure 8D, E&F). This resulted in stable blinking of the fluorophore throughout the whole acquisition, and identification of the actin nanostructures in the presynapse (Figure 8F). However, as earlier mentioned, it is interesting to try other labelling strategies, such as nanobodies, to reduce the linkage error and enhance the accessibility of the binding sites (de Beer & Giepmans, 2020).

Therefore, an anti-ALFA nanobody that was coupled to docking strand 3 to perform DNA-PAINT was used to obtain a more detailed image of the presynaptic actin nanostructure (Figure 8G, H&I). Blinking of fluorophores in DNA-PAINT is caused by binding of the imager strand to the docking strand. This intrinsically transient fluorescence does not allow to visualize the fluorescence of tagged neurons using regular epifluorescence, impeding the identification of knock-in neurons in the culture. It was thus impossible to find synapses between axons of knock-in neurons and dendrites of non-knock-in neurons. Hence, we used a 'double tag': actin was tagged with both FLAG and ALFA. The FLAG-tag was stained by an anti-FLAG primary antibody in combination with the appropriate secondary antibody that was coupled to Alexa Fluor 488 for regular epifluorescence and tagged neurons identification, while the ALFA-tag was stained using a DNA-PAINT nanobody.

The staining of the FLAG-tag allowed us to find synapses between knock-in and non-knock-in neurons (Figure 8G&H). Finally, the super-resolved image of the ALFA-tag revealed the three actin nanostructures in natural synapses (Figure 8I), suggesting that the actin nanostructures that are found in the bead-induced model are also present in 'natural' synapses. However, the number of blinking events was rather low.

Lastly, an anti-ALFA nanobody that was coupled to docking strand F3 to perform DNA-PAINT was used to image a 3X ALFA-tag, meaning that the N-terminus of b-actin was tagged three times with the ALFA tag to obtain more blinking events (Figure 8J, K&L). To overcome the earlier mentioned problem with the identification of the knock-in neurons while using DNA-PAINT, the nanobody was coupled to an Atto 488 fluorophore, in addition to the F3 docking strand for DNA-PAINT. The super-resolved image of the 3X ALFA-tag resulted in the identification of the actin mesh, rails, and corrals. The finding of the three actin nanostructures with these different labelling strategies suggest that the bead-induced presynaptic model gives a valid representation of the presynaptic actin structure.

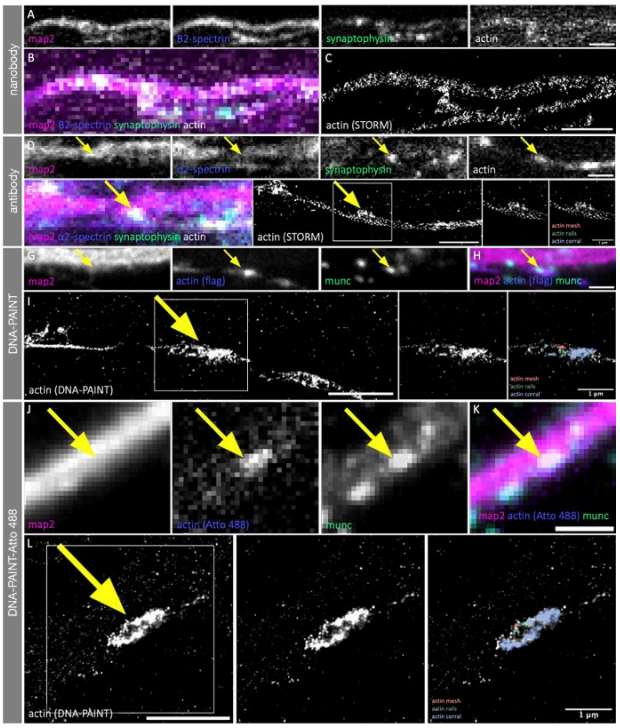

Figure 8. Three distinct nanostructures present in ALFA-actin presynapses labelled with a primary and secondary antibody, and DNA-PAINT nanobodies. (Figure on the next page >.)
(A) Diffraction limited image of map2 (magenta), b2-spectrin (purple), synaptophysin (green) and actin (white), and (B) an overlay of the four images. (C) STORM image of actin that is endogenously tagged with ALFA. ALFA is labelled with a nanobody anti-ALFA coupled to Alexa Fluor 647. (D) Diffraction limited image of map2 (magenta), α2-spectrin (purple), synaptophysin (green) and actin (white), and (E) an overlay of the four images. (F) STORM images of actin that is endogenously tagged with ALFA. ALFA is labelled with an anti-ALFA primary antibody with the appropriate secondary antibody coupled to Alexa Fluor 647. The zooms on the right are indicated in the image on the left. In the right zoom, the actin mesh (red), rails (green), and corral (blue) are indicated. (G) Diffraction limited images of map2 (magenta), flag (purple), and munc (green), and (H) an overlay of the three images. (I) DNA-PAINT image of actin that is endogenously tagged with a 'double tag' of FLAG and ALFA. ALFA is labelled with a nanobody anti-ALFA that is coupled to docking strand 3, and the I3 imager coupled to Atto 655. The zooms on the right are indicated in the image on the left. In the right zoom, the actin mesh (red), rails (green), and corral (blue) are indicated. (J) Diffraction limited images of map2 (magenta), actin (purple, labelled with the Atto 488 fluorophore that is on the nanobody), and munc (green), and (K) an overlay of the three images. (L) DNA-PAINT image of actin that is endogenously tagged with a 3X ALFA-tag. ALFA is labelled with a nanobody anti-ALFA that is coupled to docking strand F3, with an F3 imager coupled to Atto 643. The zooms on the right are indicated in the image on the left. In the right zoom, the actin mesh (red), rails (green), and corral (blue) are indicated. The arrows indicate a synapse between an axon of a knock-in (KI) neuron, and a dendrite of a non-KI neuron. Scale bars = 2 mm.

Discussion

In this work, we first show that the three presynaptic actin nanostructures found by Bingham et al. (2022) are present in actin enriched, actin non-enriched, excitatory, and inhibitory bead-induced presynapses. Furthermore, it is confirmed that the nanostructures are also present in 'natural' synapses that are formed between an axon and a dendrite. As described earlier, presynaptic actin is difficult to observe due to the apposed dense postsynaptic actin cluster. Therefore, CRISPR-Cas9 is used to endogenously tag β-actin (Gao et al., 2019). Infection or transfection with CRISPR-Cas9 constructs led to a small number of neurons on a coverslip expressing tagged β-actin, resulting in synapses with an endogenously tagged β-actin presynaptic compartment, and a non-tagged postsynaptic compartment. The imaging of the actin tag was pushed forward using different labelling strategies, such as antibodies, nanobodies, and DNA-PAINT nanobodies. b-actin endogenously tagged with an ALFA-tag, labelled with an antibody, or a DNA-PAINT nanobody revealed the existence of distinct actin nanostructures in 'natural' synapses (Götzke et al., 2019).

We thus showed that the actin cytoskeleton structure of the bead-induced presynapses resembles the actin structure of 'natural' synapses. Confirmation of the existence of the three presynaptic actin nanostructures in 'natural' synapses verified the bead-induced presynaptic model as an appropriate model to mimic presynaptic compartments without the need for postsynaptic partners. To further verify the bead-induced presynaptic model, future research could focus on quantifying the presence or absence of the three actin nanostructures, to see if the structures are present in the same quantities in the bead-induced and 'natural' synapses. This could be done manually as it is done in the paper by Bingham et al. (2022) and this work. However, it would be valuable to search for a way to automatically quantify the actin mesh, rails, and corrals, with for example a segmentation and classification algorithm based on deep learning.

Because the presynaptic actin structure is hard to observe in the presence of the dense postsynaptic actin cluster, the bead-induced presynaptic model offers a way to overcome this imaging problem. Verification of this bead-induced presynaptic model is hopefully the starting point for future research aiming to unravel the regulation of presynaptic actin structures in response to neuronal activity or pathological contexts such as neurodegeneration.

This thesis also aimed to push super-resolution presynaptic actin imaging further, by comparing different endogenous tags for actin and labelling strategies. Endogenous tagging of actin is crucial to observe presynaptic actin, because here again it is necessary to circumvent the imaging of the apposed postsynaptic actin cluster. After experimenting with GFP-, HA-, Spot- (Proteintech, n.d.; Virant et al., 2018), and ALFA-tags (Götzke et al., 2019), the ALFA-tag in combination with a nanobody suitable for DNA-PAINT was the most appropriate approach to image presynaptic actin. Nevertheless, to use the DNA-PAINT nanobody for labelling of endogenously tagged actin, two epifluorescent channels are necessary to observe actin: one channel for the super-resolved DNA-PAINT imaging, and another channel to identify the knock-in cells.

This is unfortunate, considering that one only has four channels to label different structures, and it would be convenient to label five structures (dendrites, axons, presynapses, actin, and knock-in cells) to find regions of interest. Hence, to push the imaging of presynaptic actin in 'natural' synapses even further, one could consider a labelling strategy that only consumes one channel, but performs as well as DNA-PAINT, regarding its small size and resistance to bleaching (Jimenez et al., 2020; Lelek et al., 2021).

The discovery of the three actin nanostructures in 'natural' synapses allows us to speculate about the possible function of actin at the presynapse. First, it is thought that the actin mesh hinders exocytosis, as well as facilitates the process (Li et al., 2018). The actin mesh can capture a vesicle and subsequently translocate it towards the exocytosis site. Upon excitation, the concentration of the actin mesh at the active zone decreases and actin facilitates the exocytosis event (Li et al., 2018; Wu & Chan, 2022). Besides, the actin mesh is proposed to be involved in RRP replenishment, by removing proteins from the active zone directly after RRP depletion (Wu & Chan, 2022). This active zone clearance facilitates RRP replenishment by making the way free for new vesicles to arrive at the membrane for exocytosis. This seems contradictory to the actin barrier-hypothesis. However, it is thought that this RRP replenishment occurs directly after RRP depletion, whereas actin functions as a barrier in a longer timescale. Besides, the actin mesh is also suspected to be involved in endocytosis, by regulating pit formation and membrane tension (Wu & Chan, 2022). These hypotheses point out that the actin mesh is a dynamic structure that serves several different functions in the vesicle endo- and exocytosis cycle.

Interestingly, a study in mouse hippocampal neurons found that there was no actin mesh present at the active zone (Jing et al., 2022). Supposing that the actin mesh is not present at the active zone, several hypotheses about the mesh function, as for example the exocytosis facilitation, are challenged. Since the actin mesh is a rather small structure, STED (stimulated emission depletion) microscopy, with a typical resolution of approximately 60 nm (Jacquemet et al., 2020), that is used by Jing et al. (2022) might not offer the resolution that is required to observe the actin mesh. Besides, in this work the active zone marker is not super resolved, making it hard to define how the actin mesh relates to the active zone precisely. Thus, the contrast in findings might be explained by methodological differences. However, since the actin mesh seems to be a highly dynamic structure that serves different functions during the endo- and exocytotic cycle, it could also be explained by a difference in time in the endo-/exocytosis cycle. It would be interesting to research the presynaptic actin cytoskeleton during different stages of the vesicle endo- and exocytosis cycle.

Second, the actin rails are thought to be involved in synaptic vesicle trafficking from and to the RP. Rails-like structures between the active zone and the RP have been found before (Siksou et al., 2007). Besides, it is found that administration of Latrunculin A, a toxin that stimulates depolymerization of actin, slowed down recovery after repetitive stimulation (Sakaba & Neher, 2003). This suggested that presynaptic actin polymerization is involved in vesicle recruitment to the active zone during repetitive stimulation. This might be through the earlier mentioned active zone clearance, but the discovery of the actin rails might suggest that polymerized actin is also involved in RRP replenishment by facilitating trafficking of vesicles.

Conclusively, there are clues that the actin rails are involved in vesicular transport in the presynapse between the RP and RRP.

Nevertheless, to draw reliable conclusions about the function of the presynaptic actin trails, more research is needed. An interesting start would be 2-color STORM in which actin as well as synaptic vesicles are super-resolved. This will allow us to determine if synaptic vesicles colocalize with the actin rails. Stimulation of the synapses could then show us if the effect of activity on the localization of the actin rails, presynaptic actin nanostructures in general, and synaptic vesicles.

Lastly, the actin corrals that are surrounding the presynapse, are thought to serve a function in maintenance of the RP (Sankaranarayanan et al., 2003). It was found that actin is surrounding synaptic vesicles in the periphery of the presynapse. Moreover, disruption of presynaptic actin affected the concentration of synaptic vesicle associated proteins as synapsin. This suggests that actin might act as a scaffolding protein to regulate the RP. Additionally, there are studies that found that actin might be involved in endocytosis (Bloom et al., 2003; Del Signore et al., 2021; Jing et al., 2022). Interestingly, stimulation of the synapse resulted in actin clustering in the presynaptic compartment in the area surrounding the presynaptic compartment (Bloom et al., 2003; Del Signore et al., 2021; Sankaranarayanan et al., 2003). A few minutes after stimulation this actin enrichment was abolished. This might explain the difference in corral size in actin enriched and non-enriched synapses: actin enriched synapses that relate to enlarged corrals might have just now been activated, resulting in actin accumulation, whereas actin non-enriched synapses with smaller corrals have not been recently activated.

These different functions of the actin nanostructures could explain the contradictory results regarding actin function in the presynapse. Distortion of the polymerization of actin could on short term lead to more vesicle release into the synaptic cleft, due to the absence of the actin mesh. However, in the long term it could lead to less vesicle release because trafficking of vesicles via the actin rails between the RP and RRP is hindered, and the RP is not maintained by the actin corral.

In conclusion, this thesis found that the three recently described presynaptic actin nanostructures are present in actin enriched, actin non-enriched, inhibitory and excitatory bead-induced synapses. Furthermore, this thesis provides support for the bead model as a presynaptic model, by confirming the existence of the actin nanostructures in ‘natural’ synapses that are formed between an axon and a dendrite. Imaging of actin in the presynaptic compartment is pushed forward, by implementing CRISPR-Cas9 genome editing to endogenously tag actin with a small ALFA-tag and using DNA-PAINT with its small linkage error and resistance to bleaching as label. This novel and unique combination of techniques allowed us to observe the presynaptic actin structure in natural synapses, that was not observed before. Hopefully, the discovery of the presynaptic actin mesh, rails and corral contributes to the understanding of the contradictory findings regarding the function of actin in the presynapse. Moreover, we hope that the contribution of this thesis to pushing imaging strategies for presynaptic actin is the start for future research that aims to unravel the presynaptic actin structure in various physiological and pathological conditions, as well as providing a basis to optimize the super-resolution imaging of other endogenously tagged targets in neurons.

Acknowledgements

I thank Fanny Boroni-Rueda for handling the neuronal cell culture every week and teaching me how to prepare samples for imaging. I want to thank Nicolas Jullien for the production of the plasmids and AAVs and carrying out most of the transfections/infections. Additionally, I want to thank Nicolas for teaching me how to carry out transfections/infections myself and all the molecular principles behind it. Karoline Friedl for teaching me how to work with and image DNA-PAINT samples. Theresa Wiesner, Marie-Jeanne Papandréou, and Christophe Leterrier for the feedback on my thesis and the discussions. I also want to thank Christophe Leterrier for designing the project and supervising me throughout the internship, and of course the whole NeuroCyto Lab. Christophe Leterrier and Nael Nadif Kasri for reading and grading the final version of my thesis. Lastly, I want to thank Erasmus+ and Stichting Fonds Dr. Christine Buisman for the support.

References

Bingham, D., Wernert, F., Da Costa Moura, J., Boroni-Rueda, F., van Bommel, N., Caillol, G., Papandréou, M.-J., & Leterrier, C. (2022). Distinct nano-structures support a multifunctional role of actin at presynapses. BioRxiv.

Bloom, O., Evergren, E., Tomilin, N., Kjaerulff, O., Löw, P., Brodin, L., Pieribone, V. A., Greengard, P., & Shupliakov, O. (2003). Colocalization of synapsin and actin during synaptic vesicle recycling. The Journal of Cell Biology, 161(4), 737–747. https://doi.org/10.1083/jcb.200212140

Cingolani, L. A., & Goda, Y. (2008). Actin in action: the interplay between the actin cytoskeleton and synaptic efficacy. Nature Reviews Neuroscience 2008 9:5, 9(5), 344–356. https://doi.org/10.1038/nrn2373

de Beer, M. A., & Giepmans, B. N. G. (2020). Nanobody-Based Probes for Subcellular Protein Identification and Visualization. Frontiers in Cellular Neuroscience, 14, 352. https://doi.org/10.3389/FNCEL.2020.573278/BIBTEX

Del Signore, S. J., Kelley, C. F., Messelaar, E. M., Lemos, T., Marchan, M. F., Ermanoska, B., Mund, M., Fai, T. G., Kaksonen, M., & Rodal, A. A. (2021). An autoinhibitory clamp of actin assembly constrains and directs synaptic endocytosis. ELife, 1–31. https://doi.org/10.7554/eLife.69597

Dillon, C., & Goda, Y. (2005). THE ACTIN CYTOSKELETON: Integrating Form and Function at the Synapse. Annual Review Neuroscience, 28, 25–55. https://doi.org/10.1146/ANNUREV.NEURO.28.061604.135757

Favuzzi, E., & Rico, B. (2018). Molecular diversity underlying cortical excitatory and inhibitory synapse development. Current Opinion in Neurobiology, 53, 8–15. https://doi.org/10.1016/J.CONB.2018.03.011

Gao, Y., Hisey, E., Bradshaw, T. W. A., Erata, E., Brown, W. E., Courtland, J. L., Uezu, A., Xiang, Y., Diao, Y., & Soderling, S. H. (2019). Plug-and-Play Protein Modification Using Homology-Independent Universal Genome Engineering. Neuron, 103(4), 583-597.e8. https://doi.org/10.1016/j.neuron.2019.05.047

Gentile, J. E., Carrizales, M. G., & Koleske, A. J. (2022). Control of Synapse Structure and Function by Actin and Its Regulators. Cells 2022, Vol. 11, Page 603, 11(4), 603. https://doi.org/10.3390/CELLS11040603

Götzke, H., Kilisch, M., Martínez-Carranza, M., Sograte-Idrissi, S., Rajavel, A., Schlichthaerle, T., Engels, N., Jungmann, R., Stenmark, P., Opazo, F., & Frey, S. (2019). The ALFA-tag is a highly versatile tool for nanobody-based bioscience applications. Nature Communications 2019 10:1, 10(1), 1–12. https://doi.org/10.1038/s41467-019-12301-7

Jacquemet, G., Carisey, A. F., Hamidi, H., Henriques, R., & Leterrier, C. (2020). The cell biologist's guide to super-resolution microscopy. Journal of Cell Science, 133(11). https://doi.org/10.1242/JCS.240713/VIDEO-3

Jimenez, A., Friedl, K., & Leterrier, C. (2020). About samples, giving examples: Optimized Single Molecule Localization Microscopy. In Methods (Vol. 174, pp. 100–114). Academic Press Inc. https://doi.org/10.1016/j.ymeth.2019.05.008

Jing, H., Ogunmowo, T., Raychaudhuri, S., Kusick, G. F., Imoto, Y., Li, S., Itoh, K., Chapman, E. R., Ha, T., Watanabe, S., & Liu, J. (2022). Membrane compression by synaptic vesicle exocytosis triggers ultrafast endocytosis. BioRxiv, 2022.06.12.495801. https://doi.org/10.1101/2022.06.12.495801

Kevenaar, J. T., & Hoogenraad, C. C. (2015). The axonal cytoskeleton: from organization to function. Frontiers in Molecular Neuroscience, 8(AUGUST). https://doi.org/10.3389/FNMOL.2015.00044

Klemmer, P., Meredith, R. M., Holmgren, C. D., Klychnikov, O. I., Stahl-Zeng, J., Loos, M., van der Schors, R. C., Wortel, J., de Wit, H., Spijker, S., Rotaru, D. C., Mansvelder, H. D., Smit, A. B., & Li, K. W. (2011). Proteomics, Ultrastructure, and Physiology of Hippocampal Synapses in a Fragile X Syndrome Mouse Model Reveal Presynaptic Phenotype * □ S. Journal of Biological Chemistry, 286, 25495–25504. https://doi.org/10.1074/jbc.M110.210260

Korobova, F., & Svitkina, T. (2010). Molecular Architecture of Synaptic Actin Cytoskeleton in Hippocampal Neurons Reveals a Mechanism of Dendritic Spine Morphogenesis. Molecular Biology of the Cell, 21, 165–176. https://doi.org/10.1091/mbc.E09

Lelek, M., Gyparaki, M. T., Beliu, G., Schueder, F., Griffié, J., Manley, S., Jungmann, R., Sauer, M., Lakadamyali, M., & Zimmer, C. (2021). Single-molecule localization microscopy. Nature Reviews Methods Primers, 1(1). https://doi.org/10.1038/S43586-021-00038-X

Leterrier, C. (2021a). A Pictorial History of the Neuronal Cytoskeleton. https://doi.org/10.1523/JNEUROSCI.2872-20.2020

Leterrier, C. (2021b). Putting the axonal periodic scaffold in order. In Current Opinion in Neurobiology (Vol. 69, pp. 33–40). Elsevier Ltd. https://doi.org/10.1016/j.conb.2020.12.015

Leterrier, C., Dubey, P., & Roy, S. (2017). The nano-architecture of the axonal cytoskeleton. Nature Reviews Neuroscience, 18(12), 713–726. https://doi.org/10.1038/nrn.2017.129ï

Li, P., Bademosi, A. T., Luo, J., & Meunier, F. A. (2018). Actin Remodeling in Regulated Exocytosis: Toward a Mesoscopic View. Trends in Cell Biology, 28(9), 685–697. https://doi.org/10.1016/J.TCB.2018.04.004

Lucido, A. L., Suarez Sanchez, F., Thostrup, P., Kwiatkowski, A. V, Leal-Ortiz, S., Gopalakrishnan, G., Liazoghli, D., Belkaid, W., Lennox, R. B., Grutter, P., Garner, C. C., & Colman, D. R. (2009). Rapid Assembly of Functional Presynaptic Boutons Triggered by Adhesive Contacts. https://doi.org/10.1523/JNEUROSCI.1381-09.2009

Nishizono, H., Yasuda, R., & Laviv, T. (2020). Methodologies and Challenges for CRISPR/Cas9 Mediated Genome Editing of the Mammalian Brain. Frontiers in Genome Editing, 0, 18. https://doi.org/10.3389/FGEED.2020.602970

Ovesný, M., Křížek, P., Borkovec, J., Švindrych, Z., & Hagen, G. M. (2014). ThunderSTORM: a comprehensive ImageJ plug-in for PALM and STORM data analysis and super-resolution imaging. Bioinformatics, 30(16), 2389–2390. https://doi.org/10.1093/BIOINFORMATICS/BTU202

Proteintech. (n.d.). First Peptide-tag specific Nanobody applied in super resolution microscopy (SRM) | Proteintech Group. Retrieved February 27, 2023, from https://www.ptglab.com/news/blog/first-peptide-tag-specific-nanobody-applied-in-super-resolution-microscopy-srm/
Ries, J. (2020). SMAP: a modular super-resolution microscopy analysis platform for SMLM data. In Nature Methods (Vol. 17, Issue 9, pp. 870–872). Nature Research. https://doi.org/10.1038/s41592-020-0938-1

RStudio Team. (2020). RStudio: Integrated Development for R. http://www.rstudio.com/

Rust, M. J., Bates, M., & Zhuang, X. (2006). Sub-diffraction-limit imaging by stochastic optical reconstruction microscopy (STORM). Nature Methods, 3(10), 793–795. https://doi.org/10.1038/nmeth929]

Sakaba, T., & Neher, E. (2003). Involvement of Actin Polymerization in Vesicle Recruitment at the Calyx of Held Synapse. The Journal of Neuroscience, 23(3), 837–846. https://doi.org/0270-6474/03/230837-10$15.00/0

Sankaranarayanan, S., Atluri, P. P., & Ryan, T. A. (2003). Actin has a molecular scaffolding, not propulsive, role in presynaptic function. Nature Neuroscience 2003 6:2, 6(2), 127–135. https://doi.org/10.1038/nn1002

Schindelin, J., Arganda-Carreras, I., Frise, E., Kaynig, V., Longair, M., Pietzsch, T., Preibisch, S., Rueden, C., Saalfeld, S., Schmid, B., Tinevez, J. Y., White, D. J., Hartenstein, V., Eliceiri, K., Tomancak, P., & Cardona, A. (2012). Fiji: an open-source platform for biological-image analysis. Nature Methods 2012 9:7, 9(7), 676–682. https://doi.org/10.1038/nmeth.2019

Siksou, L., Rostaing, P., Lechaire, J.-P., Boudier, T., Ohtsuka, T., Fejtová, A., Kao, H.-T., Greengard, P., Gundelfinger, E. D., Triller, A., & Marty, S. (2007). Three-Dimensional Architecture of Presynaptic Terminal Cytomatrix. https://doi.org/10.1523/JNEUROSCI.1773-07.2007

Sousa, V. L., Bellani, S., Giannandrea, M., Yousuf, M., Valtorta, F., Meldolesi, J., & Chieregatti, E. (2009). α-Synuclein and its A30P mutant affect actin cytoskeletal structure and dynamics. Molecular Biology of the Cell, 20(16), 3725–3739. https://doi.org/10.1091/MBC.E08-03-0302/ASSET/IMAGES/LARGE/ZMK0160991500011.JPEG

Speiser, A., Müller, L. R., Hoess, P., Matti, U., Obara, C. J., Legant, W. R., Kreshuk, A., Macke, J. H., Ries, J., & Turaga, S. C. (2021). Deep learning enables fast and dense single-molecule localization with high accuracy. Nature Methods, 18(9), 1082–1090. https://doi.org/10.1038/s41592-021-01236-x

Star, E. N., Kwiatkowski, D. J., & Murthy, V. N. (2002). Rapid turnover of actin in dendritic spines and its regulation by activity. Nature Neuroscience, 5(3), 239–246. https://doi.org/10.1038/nn811

Südhof, T. C. (2021). The cell biology of synapse formation. Journal of Cell Biology, 220(7). https://doi.org/10.1083/JCB.202103052/212258

Traenkle, B., & Rothbauer, U. (2017). Under the microscope: Single-domain antibodies for live-cell imaging and super-resolution microscopy. Frontiers in Immunology, 8(AUG), 1030. https://doi.org/10.3389/FIMMU.2017.01030/BIBTEX

Virant, D., Traenkle, B., Maier, J., Kaiser, P. D., Bodenhöfer, M., Schmees, C., Vojnovic, I., Pisak-Lukáts, B., Endesfelder, U., & Rothbauer, U. (2018). A peptide tag-specific nanobody enables high-quality labeling for dSTORM imaging. Nature Communications 2018 9:1, 9(1), 1–14. https://doi.org/10.1038/s41467-018-03191-2

Wu, L. G., & Chan, C. Y. (2022). Multiple Roles of Actin in Exo- and Endocytosis. Frontiers in Synaptic Neuroscience, 14. https://doi.org/10.3389/FNSYN.2022.841704

Wu, X. S., Lee, S. H., Sheng, J., Zhang, Z., Zhao, W. D., Wang, D., Jin, Y., Charnay, P., Ervasti, J. M., & Wu, L. G. (2016). Actin Is Crucial for All Kinetically Distinguishable Forms of Endocytosis at Synapses. Neuron, 92(5), 1020–1035. https://doi.org/10.1016/J.NEURON.2016.10.014

Xu, K., Zhong, G., & Zhuang, X. (2013). Actin, spectrin, and associated proteins form a periodic cytoskeletal structure in axons. Science, 339(6118), 452–456. https://doi.org/10.1126/science.1232251

Zhang, W., & Benson, D. L. (2002). Developmentally regulated changes in cellular compartmentation and synaptic distribution of actin in hippocampal neurons. Journal of Neuroscience Research, 69(4), 427–436. https://doi.org/10.1002/JNR.10313